analytical chemistry

Article

Cite This: *Anal. Chem.* XXXX, XXX, XXX−XXX

pubs.acs.org/ac

Cascade Amplification-Mediated In Situ Hot-Spot Assembly for MicroRNA Detection and Molecular Logic Gate Operations

Sha Yu,[†] Yingying Wang,[†] Li-Ping Jiang,*[,†] Sai Bi,*[,‡] and Jun-Jie Zhu[†]

[†]State Key Laboratory of Analytical Chemistry for Life Science, School of Chemistry and Chemical Engineering, Nanjing University, Nanjing, Jiangsu 210093, China

[‡]Collaborative Innovation Center for Marine Biomass Fiber, Materials and Textiles of Shandong Province, College of Chemistry and Chemical Engineering, Laboratory of Fiber Materials and Modern Textiles, the Growing Base for State Key Laboratory, Qingdao University, Qingdao 266071, China

Supporting Information

ABSTRACT: MicroRNAs (miRNAs) play important roles in many biological processes and are associated with various diseases, especially cancers. Combination of technological developments such as nanomaterials, functional enzyme-mediated reactions, and DNA nanotechnology holds great potential for high-performance detection of miRNAs in molecular diagnostic systems. In this work, we have fabricated a cascade signal amplification platform through integrating duplex-specific nuclease (DSN)-assisted target recycling with catalytic hairpin assembly (CHA) reaction for the detection of microRNA-141 (miR-141). The target recycling process driven by DSN results in highly amplified translation of target miRNA to single-stranded connector DNA fragments. The CHA reaction is further initiated by connector DNAs using hairpin-modified gold nanoparticles (HP-AuNPs) as the sensing unit, leading to the formation of AuNP network architecture on the electrode for electrochemical and photoelectrochemical detection of miR-141 in signal-on and signal-off modes, respectively. The developed electrochemical biosensor exhibits a detection limit down to 25.1 aM miR-141 (60 copies in 4 μL sample) and excellent selectivity to discriminate a single base-mismatched sequence and other miRNAs. This assay is also applied to the determination of miR-141 in total RNAs extracted from human breast cancer cells (MDA-MB-231), confirming the applicability of this method for absolute quantification of specific miRNAs in real-world samples. Furthermore, two-input AND and INHIBIT (INH) logic gates are constructed to detect miRNAs. In particular, the AND gate achieves cell-specific gate activation based on expression profiles of miR-141 and microRNA-21 (miR-21). Therefore, our proposed cascade amplification platform has great potential applications in miRNA-related clinical diagnostics and biochemical research.

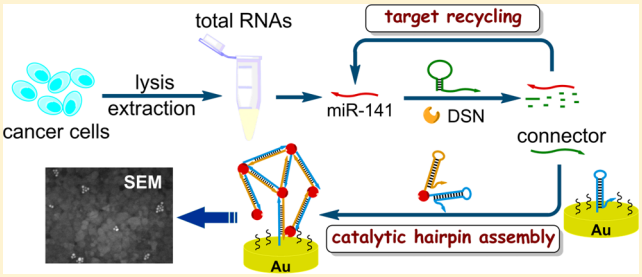

MicroRNAs (miRNAs) are a class of endogenous noncoding ribonucleic acids with lengths of 18−25 nucleotides (nt) that play important roles in physiological and pathological processes, such as hematopoietic differentiation, cell proliferation, genetic expression, and metabolism.[1] It has been found that aberrant expression of miRNAs is closely associated with a variety of diseases, especially cancers.[2] For example, miR-141 is abnormally expressed in prostate cancer,[3] and miR-21 has been found to be overexpressed in many types of cancers.[4] MicroRNAs thus have been considered as potential biomarkers in diagnosis, prognosis, and therapy monitoring of cancers. Therefore, the development of strategies for sensitive and selective detection of miRNAs is in urgent demand for biomedical research, especially for early diagnosis of cancers as well as discovery of new targets for drugs.

So far, various analytical methods have been proposed for identification and quantification of miRNAs, such as Northern blotting,[5] microarray,[6] and polymerase chain reaction (PCR)-based methods.[7] However, due to the unique characteristics of miRNAs, including short length, low cellular abundance, high sequence homology, and easy degradability,[8] these methods often suffer from the shortcomings of low sensitivity, poor specificity, and sophisticated operations. Alternatively, isothermal amplification strategies have attracted great interest in miRNA analysis.[9,10] Based on the mechanism of signal amplification, these methods can be mainly classified into two types: nuclease-assisted reactions and enzyme-free reactions. In general, the nuclease-assisted methods often involve target recycling processes induced by different nucleases, such as endonuclease,[11] exonuclease,[12] ligase,[13] and duplex-specific nuclease (DSN).[14−16] Additionally, polymerase-directed rolling circle amplification (RCA) has also been reported for miRNA detection.[17,18] For enzyme-free methods, toehold-mediated strand displacement (TMSD) reactions that are independent of enzymes have become increasingly attractive for signal amplification of miRNA with dynamic properties.[19,20] The

Received: November 28, 2017
Accepted: March 19, 2018

DOI: 10.1021/acs.analchem.7b04930
Anal. Chem. XXXX, XXX, XXX−XXX

representative TMSD-based amplification works are hybridization chain reaction (HCR)[21,22] and catalytic hairpin assembly (CHA),[23] which were proposed by Pierce's group and have been versatilely applied to quantitative analysis of miRNAs by colorimetric,[24] fluorescent,[25] and electrochemical assays.[26,27] In particular, electrochemical biosensors, especially label-free strategies, have attracted considerable interest because of the advantages of easy operation, rapid detection, low cost, and high repeatability.[47,48] Given the unique characteristics of miRNAs and the practical significance of miRNA analysis, it is still a great challenge to combine diverse isothermal amplification strategies with different detection techniques for accurate, sensitive, and selective determination of miRNAs.

It has been found that one disease is often associated with more than one biomarker, and their logical relationship is often related to different disease states.[28,29] To address this issue, molecular logic gates, which use biological molecules as input and output signals to perform Boolean logic, have been developed for controlling biological progress at the molecular level, such as multiplexed biomarker detection, disease diagnosis, and gene regulation.[30,31] So far, various molecular logic gates have been devised that relied on not only enzyme catalysis[32−34] but also DNA TMSD-based reactions,[35,36] holding great promise for molecular diagnosis and therapy. However, due to the low concentration of analyte in biological samples and certain signal interferences in heterogeneous systems, the application of molecular logic gates in real samples has been rarely reported.

Herein, we have demonstrated a cascade amplification strategy through combining DSN-assisted target recycling amplification with TMSD-based CHA reaction to self-assemble gold nanoparticle (AuNP) networks in situ as hot spots, achieving label-free electrochemical and photoelectrochemical biosensing of miR-141 with high sensitivity and selectivity. On the basis of the prototype, we further design modular AND and INH Boolean logic gates using two miRNAs as the inputs, which is successfully applied to logically analyze miRNAs in different cancer cells.

EXPERIMENTAL SECTION

Preparation of DNA Hairpin-Modified Gold Nanoparticles. Briefly, 30 mL of trisodium citrate (38.8 mM) was added to 1% $HAuCl_4$ solution under vigorous stirring. The solution was heated for 15 min and then naturally cooled to room temperature. The color of the solution changed from pale yellow to deep red, and finally it was stored at 4 °C until use. As-prepared AuNPs with an average diameter of 13 nm were characterized by transmission electron microscopy (TEM) and dynamic light scattering (DLS). The extinction coefficient of 13 nm AuNPs is 2.7×10^8 $M^{-1}\cdot cm^{-1}$ at 520 nm,[37] and the concentration of AuNP solution was determined to be 4.2 nM by UV−vis measurement.

AuNPs were modified with thiol-labeled DNA hairpins H2 and H3 as follows. First, the colloid solution of AuNPs was filtered through a 0.22 μm membrane, followed by pretreatment with ∼0.05 wt % sodium dodecyl sulfate (SDS) to increase their stability. Meanwhile, 75 μL of thiol-labeled H2 and H3 (1.5 μM each) was activated by 2.25 μL of tris(2-carboxyethyl)phosphine (TCEP; 10 mM, pH 5.2) for 1 h, respectively. The activated hairpins were then mixed with 150 μL of AuNPs. After incubation for 16 h at room temperature, the resulting colloid solution was salted with 33 μL of NaCl (1 M), and the mixture was allowed to stand for 24 h. To remove excess H2 and H3, the solution was purified by centrifuging for 30 min at 12000*g* three times. The resulting hairpin-modified gold nanoparticles (HP-AuNPs) were finally redispersed in a solution of tris(hydroxymethyl)aminomethane hydrochloride (Tris-HCl) and ethylenediaminetetraacetic acid (EDTA) (known as TE buffer) and stored at 4 °C for further use. The ratio of AuNPs/H2/H3 was calculated to be 1/96/64 (see Supporting Information).

Total RNA Extraction. All cell types were cultured in six-well plates, followed by washing twice with ice-cold phosphate-buffered saline solution (pH 7.4) and adding 1 mL of ice-cold TRIpure lysis buffer (BioTeke Corp.). After incubation for 5 min at room temperature, 200 μL of trichloromethane ($CHCl_3$) was added. The mixture was then centrifuged at 12000*g* for 15 min at 4 °C. Subsequently, total RNAs were purified by extraction with 2-propanol and precipitation with ethanol, respectively. Finally, the total RNA sediment was redissolved in RNase-free water and stored at −80 °C before use.

DSN-Assisted Target Recycling Amplification. An aliquot (4 μL) of annealed DNA hairpin H1 solution (5.0 μM) was mixed with 1 μL of DSN (0.1 unit, dissolved in 25 mM Tris-HCl and 50% glycerol, pH 8.0) and 4 μL of miR-141 with different concentrations in 1× reaction buffer (50 mM Tris-HCl and 5 mM $MgCl_2$, pH 8.0) with a total volume of 10 μL. After incubation at 50 °C for 90 min, 10 μL of EDTA (10 mM) was added and the mixture was incubated at 50 °C for 5 min, followed by heating at 90 °C for 20 min to completely inactivate the DSN activity and cooling to room temperature slowly. The resultant products of the DSN-assisted target recycling reaction were analyzed by nondenaturing 12% polyacrylamide gel electrophoresis (PAGE) in 1× TBE solution consisting of Tris (40 mM), acetic acid (20 mM), and EDTA (1 mM) (pH 8.3) at 150 V for 40 min. After staining and water eluting, the resulting gel was imaged.

Electrochemical Detection of miR-141. First, the gold disk electrode with diameter 4 mm was cleaned by immersion in piranha solution (a mixture of 98% H_2SO_4 and 30% H_2O_2 at a volume ratio of 3:1) for at least 30 min, followed by rinsing thoroughly with ultrapure water. Then the gold electrode was polished with 0.3 and 0.05 μm alumina oxide slurries for 5 min, respectively, to obtain a mirrorlike surface. The resulting electrode was washed by sonication in ethanol and ultrapure water for 5 min, respectively, to remove residual alumina powder. The electrode was then electrochemically cleaned through successive scans between −0.2 and +1.6 V in fresh H_2SO_4 (0.5 M) until a stable cyclic voltammogram (CV) was obtained with a scan rate of 0.1 V/s. The cleaned gold electrodes were rinsed with RNase-free water and blown dry with nitrogen.

Prior to immobilization of H2 onto the pretreated gold electrode, 200 μL of thiol-modified H2 (0.1 μM) was treated with 0.2 μL of TCEP (10 mM, pH 5.2) for 1 h at room temperature to reduce residual disulfide bonds. Then 50 μL of H2 (0.1 μM) was dropped onto the surface of gold electrode and incubated for 16 h at 4 °C. The resulting electrode was washed with ultrapure water twice and subsequently immersed into 6-mercapto-1-hexanol (MCH) solution (1 mM) for 1 h. After the electrode was washed with ultrapure water twice, 5 μL of the above DSN-assisted reaction products and 10 μL of HP-AuNPs were dropped onto the electrode surface, and it was incubated for 1 h at 37 °C. After the electrode was washed with Tris-HCl (10 mM, pH 7.4), the electrochemical signal was

DOI: 10.1021/acs.analchem.7b04930
Anal. Chem. XXXX, XXX, XXX−XXX

recorded with differential pulse voltammetry (DPV) by scanning from +0.4 to −0.6 V (versus Ag/AgCl) in 5 mL of Tris-HCl buffer (10 mM, pH 7.4) containing $[Ru(NH_3)_6]^{3+}$ (5 μM), which was degassed with nitrogen for 15 min. The surface coverage of H2 on the gold electrode was calculated to be 0.7 pmol with a diameter of 4.0 mm (~3.4×10^{10} copies/mm^2; see Supporting Information). In addition, it has been demonstrated that, after being stored at 4 °C for 3 days, the H2-immobilized gold electrode still showed excellent reproducibility (Figure S4). Hence, the modified electrode can be prepared in batches and stored at 4 °C for further use, which thus would simplify the experimental operations and shorten the preparation time.

Logic Operations. For AND gate operation, miR-141 and miR-21 were selected as the inputs. The annealed dumbbell probe (DP) (5.0 μM) was set as the initial state (0,0). In the case of input (1,0), 4 μL of DP solution (5.0 μM) was mixed with 1 μL of DSN (0.1 unit) and 4 μL of miR-141 (10 pM) in 1× reaction buffer (50 mM Tris-HCl and 5 mM $MgCl_2$, pH 8.0) with a total volume of 10 μL. For the input (0,1), miR-21 instead of miR-141 was added. For the input (1,1), both miR-141 and miR-21 were added. The other procedures were the same as those mentioned in the sections DSN-Assisted Target Recycling Amplification and Electrochemical Detection of miR-141. For operation of the AND gate in cancer cells, 4 μL of cell lysate instead of synthesized miRNAs was added into the system. The output signals generated from different cancer cells were obtained at the same number of 10^5 cells. The INH gate was operated in the same way as the AND gate but instead using miR-141 as input 1 and a certain miRNA sequence as input 2.

RESULTS AND DISCUSSION

Principle of the Strategy. The proposed assay mainly involves two parts: (i) DSN-assisted target recycling amplification and (ii) in situ self-assembly of AuNP hot-spots on electrodes via CHA reaction (Scheme 1). The two parts are connected via the single-stranded DNA called connector that is released in part i, which thus achieves cascade amplification. In this study, we chose miR-141, an important biomarker of various human malignancies,[38] as the target and human breast cancer cells (MDA-MB-231) as the analysis model. MiR-141 extracted from cancer cells hybridizes with and unfolds DNA hairpin H1 to form a DNA/RNA heteroduplex. It has been demonstrated that DSN has a strong preference for cleaving DNA duplex with more than 10 base pairs (bp) or DNA in DNA/RNA hybrids, while little activity against single-stranded DNA or RNA was seen.[39] Thus, upon formation of miR-141/H1 hybrid, DSN selectively hydrolyzes the target-binding part of H1, resulting in the release of intact miR-141 that is recycled to hybridize with another H1 and initiate a new cycle of DSN cleavage reaction. Thus, one target miRNA can cleave numerous H1 hairpins during the hybridization/DSN incubation, leading to target recycling amplification (part i). Meanwhile, massive connector DNAs that are previously caged in H1 are also released to initiate the following CHA reaction for self-assembly of AuNP hot spots on the electrode (part ii). Then the resultant products containing connector DNAs are introduced onto the H2-immobilized electrode, which initiates the opening of H2 and the formation of a connector/H2 intermediate via TMSD reaction. After that, both H2- and H3-modified AuNPs (HP-AuNPs) are added, leading to the interaction between H3 (on the AuNPs) and the newly exposed single-stranded region of H2 (on the electrode) through a secondary TMSD reaction. During this process, H2/H3 hybrid is formed on the electrode, accompanied by the displacement of connector for catalyzing a next round of CHA between H2 and H3, resulting in the self-assembly of AuNP networks on the electrode surface. Electrochemical detection is achieved by immersing the electrode in $[Ru(NH_3)_6]^{3+}$ (RuHex) solution. As a result, a large number of positively charged RuHex bind to the anionic phosphate of the H2/H3 duplex through electrostatic interaction, eventually generating a remarkably amplified electrochemical signal for label-free quantification of miR-141 in a signal-on mode. The electrochemical signal is measured by DPV. In contrast, in the absence of target miR-141, since H1 cannot be recognized and digested by DSN due to the low activity of DSN against the short stem of H1 with only 7 bp, no CHA-induced network architecture of AuNPs can be formed on the electrode. Thus, a weak DPV signal is detected. Taking advantage of the high amplification efficiency of DSN-assisted target recycling and CHA reaction, the proposed method can be used for highly sensitive determination of miRNAs in clinical applications.

It should be noted that since DSN can also cleave double-stranded DNA with more than 10 bp, a heating process is carried out after the DSN-assisted target recycling amplification step to inactivate the DSN, followed by an annealing process to ensure that the unreacted H1 is still in the stem−loop hairpin structure. In addition, in comparison with the biosensing platform fabricated through a one-step method (directly incubating the connector with H2-immobilized electrode and HP-AuNPs), a larger DPV response is observed via the adopted two-step method (incubating the connector with H2-immobilized electrode, followed by the addition of HP-AuNPs) (Figure S6). The results indicated that the sequential procedure facilitates the formation of AuNP networks on the electrode, which can effectively reduce the competition for AuNP assembly between the electrode surface and the solution. In addition, based on the proximity interaction mechanism,[40] the recycled connector should be more favorable to interact with a new H2 on the electrode than that in solution, enabling the assembly of AuNP networks on electrode surface for the following electrochemical detection.

Native Polyacrylamide Gel Electrophoretic Characterization. The reaction pathways of DSN-assisted target

Scheme 1. Schematic Illustration of Cascade Amplification of DSN-Assisted Target Recycling and CHA Reaction[a]

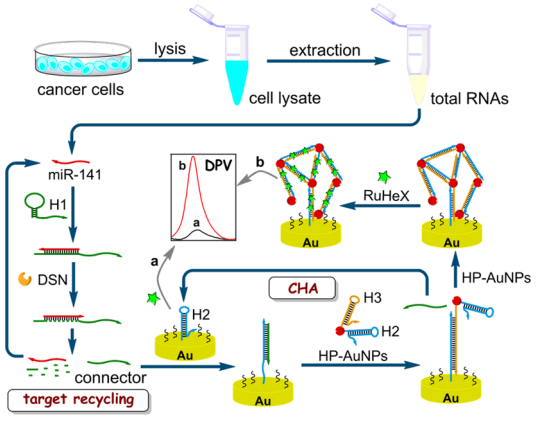

[a]For in situ self-assembly of AuNP networks on electrode for label-free electrochemical detection of miR-141 in signal-on mode.

DOI: 10.1021/acs.analchem.7b04930
Anal. Chem. XXXX, XXX, XXX−XXX

recycling amplification are confirmed by native PAGE (Figure 1). The bands of H1 (lane 1) and miR-141 (lane 3) can be

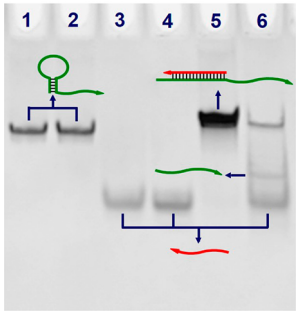

Figure 1. Native PAGE (12%) analysis of the reaction pathways of DSN-assisted target recycling amplification: (lane 1) H1; (lane 2) H1 + DSN; (lane 3) miR-141; (lane 4) miR-141 + DSN; (lane 5) H1 + miR-141; (lane 6) H1 + miR-141 + DSN.

clearly observed, even after they are treated with DSN (lanes 2 and 4, respectively). However, upon incubating the miR-141/H1 hybrid with DSN, H1 is cleaved to release the connector and intact miR-141 simultaneously (lane 6). These results successfully confirm the cleavage properties of DSN, which cannot digest miRNA and H1 with a short stem (7 bp) and can specifically hydrolyze the single-stranded DNA in the miR-141/H1 duplex. Therefore, the proposed DSN-assisted strategy provides a feasible way to fabricate a signal amplification platform.

Characterization of Gold Nanoparticle Probes. UV−vis absorption spectra of AuNPs with different states are shown in Figure S5A. The as-prepared citrate-capped AuNPs with an average diameter of 13 nm demonstrated the typical UV−vis absorption spectrum with a maximum absorption wavelength at 524 nm (curve a). Notably, two distinct absorption peaks at 524 and 260 nm are observed after AuNPs are modified with H2 and H3 (curve b). In addition, the hairpin-modified AuNPs demonstrate a more negative ζ potential than the citrate-capped AuNPs (Figure S5B). These results indicate the successful immobilization of hairpins onto the surface of AuNPs. Upon addition of connector DNA, the absorption peak of AuNPs at 524 nm is red-shifted to ~550 nm, which results from the aggregation of AuNPs triggered by the connector DNA via CHA reaction (Figure S5A, curve c).

Furthermore, the morphology and dispersity of AuNPs, HP-AuNPs, and aggregated HP-AuNPs triggered by connector DNA were characterized by TEM. Obviously, HP-AuNPs exhibit better dispersity compared with the unmodified AuNPs (Figure 2A,B). Once connector DNA is introduced, the aggregation of AuNPs is clearly observed (Figure 2C). These phenomena are consistent with the UV−vis results mentioned. In addition, the average hydrodynamic sizes of AuNPs are determined by DLS. The hydrodynamic size of the unmodified AuNPs is 13 ± 0.5 nm (Figure 2D), which increases to 18.5 ± 0.9 nm after modification with hairpins H2 and H3 to obtain HP-AuNPs (Figure 2E). Upon mixing with the connector DNAs, the particle size significantly increases to 100 ± 2.5 nm (Figure 2F), confirming the connector-triggered CHA for self-assembly of AuNP networks. All these results verify the feasibility of the proposed strategy.

Characterization of Fabricated Electrodes. Fabrication of the electrochemical biosensor was investigated by electrochemical impedance spectroscopy (EIS), which is commonly used to characterize assembly procedures of the working electrode step by step (Figure 3A). In comparison with the diameter of the semicircle in the impedance spectrum of the bare gold electrode with excellent conductivity (Figure 3A, curve a), the diameter of the semicircle in the impedance spectrum of H2-immoblized electrode increases because of the strong electrostatic repulsion between the negatively charged redox indicator ferricyanide ($[Fe(CN)_6]^{3-/4-}$) and the phosphoric acid groups of the DNA backbone (Figure 3A, curve b).[41] After blocking by MCH (Figure 3A, curve c), the semicircle diameter further increases. With the self-assembly of AuNPs on the electrode triggered by the connector via CHA reaction, a significant increase in the electrochemical impedance of the electrode is observed (Figure 3A, curve d), which is attributed to repulsion of the numerous negatively charged DNAs among the AuNP network architecture on the gold electrode by $[Fe(CN)_6]^{3-/4-}$. DPV was further used to

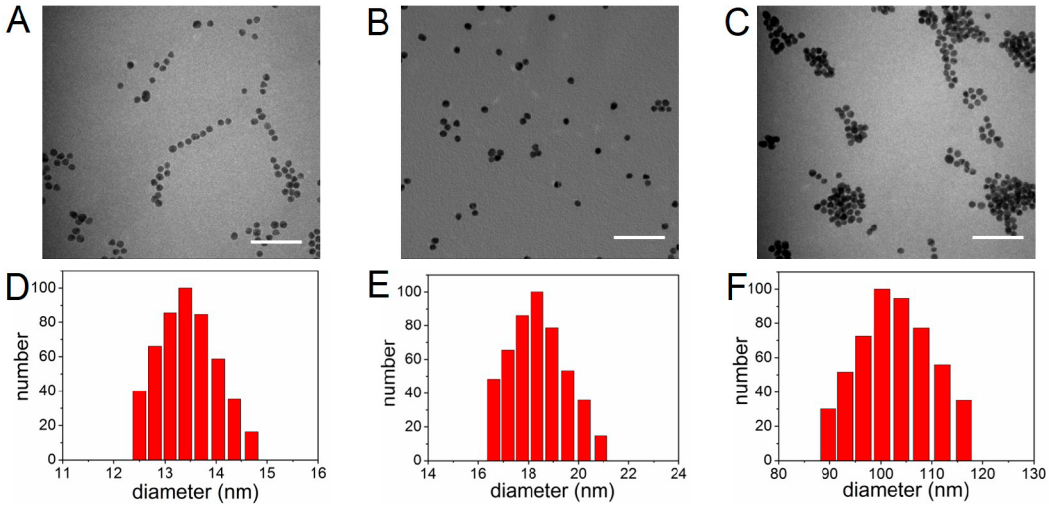

Figure 2. (A−C) TEM images and (D−F) corresponding DLS results for determining the morphology and average hydrodynamic sizes of (A, D) citrate-capped AuNPs, (B, E) HP-AuNPs in the absence of connector DNA, and (C, F) self-assembled HP-AuNPs upon incubation with connector DNA (1 nM) for 1 h. Scale bar = 100 nm.

DOI: 10.1021/acs.analchem.7b04930
Anal. Chem. XXXX, XXX, XXX−XXX

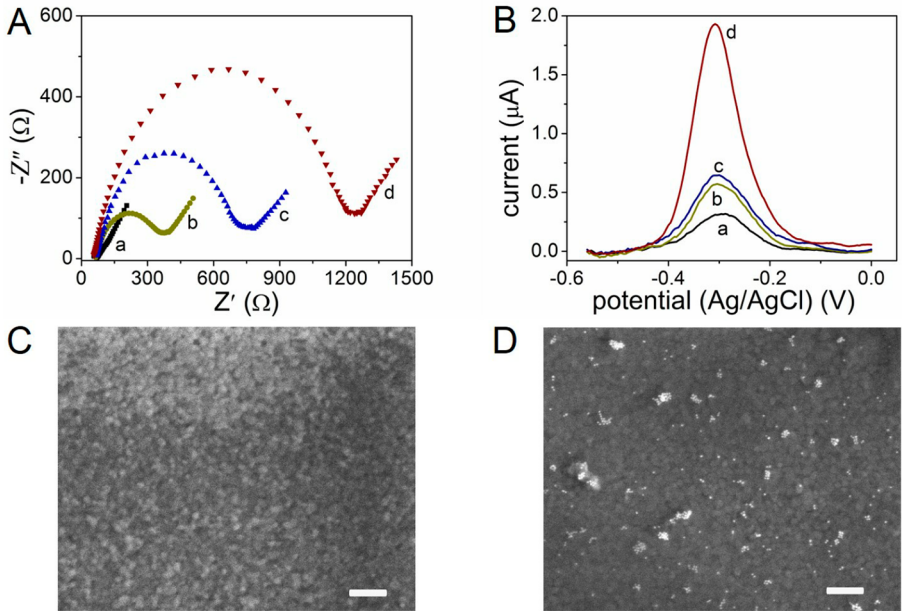

Figure 3. (A) EIS and (B) DPV curves of (a) bare gold electrode, (b) H2-modified gold electrode, (c) MCH-blocked H2-modified gold electrode, and (d) gold electrode immobilized with self-assembled HP-AuNPs triggered by connector DNA (1 pM). (C, D) SEM images of (C) H2-modified gold electrode and (D) self-assembled AuNPs on gold electrode triggered by connector DNA (1 pM). Scale bar = 200 nm.

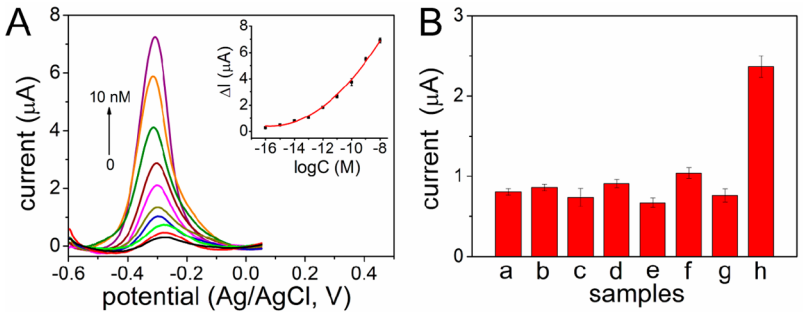

Figure 4. (A) DPV curves of RuHex in the self-assembled AuNP networks on the electrode in response to different concentrations of miR-141 via cascade amplification. From bottom to top: 0, 0.1 fM, 1 fM, 10 fM, 100 fM, 1 pM, 10 pM, 100 pM, 1 nM, and 10 nM. (Inset) Corresponding calibration curve of relative peak currents (ΔI) versus the logarithm of miR-141 concentrations. (B) Selectivity of the proposed biosensing platform toward (a) blank, (b) miR-21, (c) miR-200a, (d) miR-200b, (e) miR-200c, (f) miR-429, (g) single-base-mismatched miR-141, and (h) miR-141. The concentration of miR-141 is 10 pM, while the concentrations of other miRNAs are 1 nM. Blank sample means the condition in the absence of any miRNA. Error bars represent standard deviations from three repeated measurements.

investigate the feasibility of the electrochemical biosensor (Figure 3B). $[Ru(NH_3)_6]^{3+}$ (RuHex) is used as the signal reporter, which can bind to the anionic phosphate of DNA strands through electrostatic interaction.[42] The bare gold electrode shows a very weak DPV signal (Figure 3B, curve a), which slightly increases when the electrode is modified with H2 and MCH via Au−S bond (Figure 3B, curves b and c). In contrast, after incubation of the electrode with connector and HP-AuNPs, a remarkably increased DPV signal is recorded (Figure 3B, curve d), demonstrating the high signal amplification efficiency of CHA for electrochemical detection of miRNA.

Moreover, scanning electron microscopy (SEM) is used to verify that the connector DNA could indeed initiate the self-assembly of AuNP networks in situ on the gold substrate. As shown in Figure 3C, in the absence of connector DNA, almost no AuNP can be observed on the electrode surface, while an obvious aggregation of AuNPs occurs on the electrode when connector DNA is added into the system (Figure 3D). The results indicate the feasibility of the constructed biosensor for electrochemical detection of miRNAs through combining DSN-assisted signal amplification with CHA reaction.

Analytical Performance of Electrochemical Biosensor. The sensitivity of the proposed electrochemical biosensing platform for miR-141 quantitation was investigated by monitoring the DPV reponses of RuHex to the self-assembled AuNP networks on the electrode. As illustrated in Figure 4A, the DPV peak current gradually increases with increasing miR-141 concentration from 0 to 10 nM. The detection limit is calculated to be 25.1 aM (S/N = 3) (see Supporting Information), which is competitive with or even superior to previously reported DSN-assisted signal amplification strategies (Table S3) and other isothermal amplification electrochemical methods (Table S4) for miRNA detection. In addition, a control experiment using only H3-modified AuNPs as probes has been carried out, which obtains a detection limit of 0.81 fM (S/N = 3) that is ∼32-fold higher than that of the AuNP network-modified electrode (Figure S8). Thus, the proposed

DOI: 10.1021/acs.analchem.7b04930
Anal. Chem. XXXX, XXX, XXX−XXX

strategy of in situ self-assembly of AuNP networks on electrode via cascade amplification make a significant contribution to signal amplification and improvement of detection sensitivity. Moreover, the ultrahigh sensitivity can be attributed to low background signals for the cascade amplification method. In this assay, the following issues help to reduce the background signals. (1) Owing to the specific recognition of Watson−Crick base pairing and strong preference of DSN for cleaving DNA in DNA/RNA hybrids, the electrochemical signals are induced only by the target miRNA. Otherwise, in the absence of target miRNA, the background signal is quite weak. (2) A heating process is performed after DSN-assisted amplification to inactivate the DSN, which thus efficiently eliminates the negative effects of DSN on H2 and H3 and significantly reduces the background signals. (3) The gold electrode is blocked with MCH to avoid nonspecific adsorption, which further reduces background signals.

The selectivity of this assay was further investigated by analyzing miR-141, miR-21, miR-200a, miR-200b, miR-200c, miR-429, and single-base-mismatched miR-141 with a concentration ratio of 1:100:100:100:100:100:100 (the concentration of miR-141 is 10 pM). In this assay, H1 contains a complementary segment that is specific for miR-141, which thus exhibits excellent selectivity to well distinguish miR-141 from other miRNAs, even single-base-mismatched miR-141 (Figure 4B). In addition, to verify the applicability of this method in complex biological samples, cellular miR-141 extracted from human breast cancer cells (MDA-MB-231) is detected (Table 1). The results show good agreement with those obtained by conventional fluorescence quantitative real-time polymerase chain reaction (qRT-PCR) assay, confirming the reliability of our biosensing platform in practical applications. The proposed strategy can work well with real-life samples thanks to the ultrahigh sensitivity and excellent selectivity of the method. Besides the signal-on electrochemical biosensing strategy, this assay was versatilely applied to photoelectrochemical detection of miR-141 in a signal-off mode, which demonstrated high sensitivity with a detection limit of 0.35 pM and excellent selectivity (see Supporting Information).

Table 1. Determination of miR-141 in MDA-MB-231 Cells by the Proposed Method and by Conventional Fluorescence qRT-PCR

sample	proposed method (nM)	RSD[a] (%)	fluorescence qRT-PCR (nM)	RSD (%)
1	1.648	4.25	1.678	4.80
2	4.439	5.59	4.148	3.09

[a]Relative standard deviation.

Construction of Logic Gates. The construction of molecular logic gates for cancer cells is of great significance for the development of biological and biomedical applications.[43] For this purpose, we applied the proposal to design an AND logic gate utilizing miR-141 and miR-21 as the inputs (Figure 5A). The presence of either miR-141 or miR-21 is defined as the 1 or on state, while the state of 0 or off corresponds to no input. The output is the DPV signal of RuHex. In the constructed AND gate, when the targets miR-141 and miR-21 (the concentration of each is 10 pM) are present simultaneously, the DPV signal is higher than 1.2 μA. However, the signals are lower than 1.2 μA when one or both of the targets are absent. Therefore, we chose the signal of 1.2 μA as the threshold value. That is, the output is defined as 1 if the peak current is above the threshold of 1.2 μA, otherwise as 0 when the peak current is below 1.2 μA. In the AND gate, a dumbbell probe (DP) is designed with two loop domains that are complementary to miR-141 and miR-21, respectively. The sequence of the connector DNA is caged in the stems of DP. In the absence of any miRNA input (0,0), the connector cannot be released and thus cannot initiate the CHA to generate a DPV signal (0 or false output). When either input miR-141 (1,0) or miR-21 (0,1) is present alone, since only partial sequence of the connector DNA is liberated after miRNA recognition and DSN cleavage, no CHA can be activated and thus still a 0 output is yielded. In contrast, in the presence of both inputs miR-141 and miR-21 (1,1), the cooperative binding of the two inputs with DP activates the hydrolysis activity of

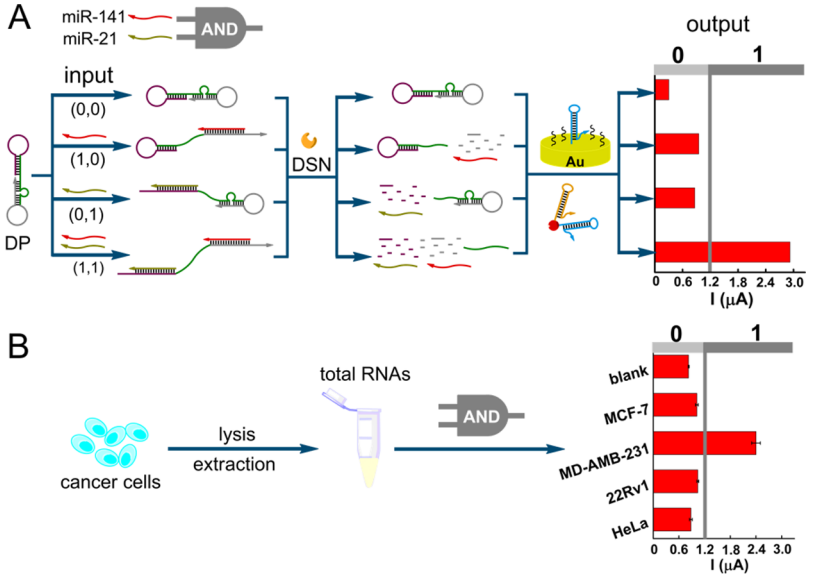

Figure 5. (A) Construction of AND logic gate using miR-21 and miR-141 as the inputs and DPV peak currents of RuHex as the outputs. The concentration of each input is 10 pM. (B) Performance of AND gate for different cancer cell lysates. The threshold is set as 1.2 μA.

DOI: 10.1021/acs.analchem.7b04930
Anal. Chem. XXXX, XXX, XXX−XXX

DSN, resulting in the release of connector DNA to initiate the CHA reaction and the generation of an amplified DPV signal (1 or true output). Thus, the true output is produced only when all the inputs exist simultaneously, which is consistent with the proper execution of a two-input AND gate.

We then demonstrated cellular activation of the AND gate in different cancer cell lysates, including 22Rv1 cells (prostate carcinoma cell lines, miR-141 overexpressed),[44] MCF-7 cells (human breast cancer cells, miR-21 overexpressed),[45] HeLa cells (cervical cancer cells, neither miR-141 nor miR-21 overexpressed),[46] and MDA-MB-231 cells (breast cancer cell lines, both miR-141 and miR-21 overexpressed) (Figure 5B).[38] As expected, the positive output appears only from the MDA-MB-231 cells compared to the other cell lysates, since both miR-141 and miR-21 are overexpressed in MDA-MB-231 cells. These results indicate reliable function of the designed AND gate, which holds great promise for preliminary analysis of miRNA expression profiles in cancerous cells.

An INH gate was also designed (Figure S11). Since only INPUT1 can produce connector DNA via DSN-assisted amplification to initiate CHA, the 1 output can only be recorded for the input state of (1,0), otherwise 0 for other input combinations of (0,0), (0,1), and (1,1). This behavior is consistent with the logic of an INH gate, in which the output of 1 is yielded only when one particular input is present. Truth tables for the AND and INH gates are presented in Figure S12.

CONCLUSION

We have developed a cascade signal amplification strategy through combining DSN-assisted target recycling and CHA to self-assemble AuNP networks in situ on the substrates, allowing electrochemical and photoelectrochemical detection of miR-141 with high sensitivity (detection limit of 25.1 aM) and specificity (single-base-mismatch discrimination). Furthermore, this assay displays the feasibility for accurate determination of miR-141 extracted from human breast cancer cell lines, which demonstrates a good correlation with the conventional qRT-PCR assay. More importantly, two-input AND and INH logic gates dependent on the presence of endogenous miRNAs are engineered for activation of electrochemical outputs. In particular, we have successfully applied the AND gate to cell-specific identification of miR-141 and miR-21. Taking advantage of the ultrahigh sensitivity, isothermal conditions, and flexible design, our versatile biosensing platform opens a promising avenue for robust, ultrasensitive, and selective detection of biomarkers of interest in biological and clinical applications.

ASSOCIATED CONTENT

Supporting Information

The Supporting Information is available free of charge on the ACS Publications website at DOI: 10.1021/acs.analchem.7b04930.

Additional text, 12 figures, and four tables, describing materials, apparatus, cell culture, photoelectrochemical detection, determination of surface coverage of DNA hairpins on gold electrode and AuNPs, reproducibility of H2-immobilized electrode, characterization of AuNP probes, electrochemical behaviors of two different incubation procedures, calculation of detection limit, comparison of DSN-assisted signal amplification assays and isothermal amplification strategies, control experiment, analytical performance of photoelectrochemical biosensor, INH gate, and truth tables (PDF)

AUTHOR INFORMATION

Corresponding Authors

*E-mail jianglp@nju.edu.cn (L.-P.J.).
*E-mail bisai11@126.com (S.B.).

ORCID

Sai Bi: 0000-0002-7305-8233
Jun-Jie Zhu: 0000-0002-8201-1285

Notes

The authors declare no competing financial interest.

ACKNOWLEDGMENTS

This work was supported by the National Natural Science Foundation of China (21335004, 21722505, and 21475057), the Special Funds of the Taishan Scholar Program of Shandong Province (tsqn20161028), and the Natural Science Foundation of Shandong Province (ZR2017JL009).

REFERENCES

(1) Git, A.; Dvinge, H.; Salmon-Divon, M.; Osborne, M.; Kutter, C.; Hadfield, J.; Bertone, P.; Caldas, C. *RNA* **2010**, *16*, 991−1006.
(2) Dong, H.; Lei, J.; Ding, L.; Wen, Y.; Ju, H.; Zhang, X. *Chem. Rev.* **2013**, *113*, 6207−6233.
(3) Sita-Lumsden, A.; Dart, D. A.; Waxman, J.; Bevan, C. L. *Br. J. Cancer* **2013**, *108*, 1925−1930.
(4) Ananta, J. S.; Paulmurugan, R.; Massoud, T. F. *Mol. Pharmaceutics* **2015**, *12*, 4509−4517.
(5) Válóczi, A.; Hornyik, C.; Varga, N.; Burgyá n, J.; Kauppinen, S.; Havelda, Z. *Nucleic Acids Res.* **2004**, *32*, e175−e181.
(6) Lee, J. M.; Jung, Y. *Angew. Chem., Int. Ed.* **2011**, *50*, 12487−12490.
(7) Moltzahn, F.; Olshen, A. B.; Baehner, L.; Peek, A.; Fong, L.; Stoppler, H.; Simko, J.; Hilton, J. F.; Carroll, P.; Blelloch, R. *Cancer Res.* **2011**, *71*, 550−560.
(8) Kaplan, M.; Kilic, T.; Guler, G.; Mandli, J.; Amine, A.; Ozsoz, M. *Biosens. Bioelectron.* **2017**, *92*, 770−778.
(9) Jia, H.; Li, Z.; Liu, C.; Cheng, Y. *Angew. Chem., Int. Ed.* **2010**, *49*, 5498−5501.
(10) Yue, S.; Zhao, T.; Bi, S.; Zhang, Z. *Biosens. Bioelectron.* **2017**, *98*, 234−239.
(11) Yin, B.-C.; Liu, Y.-Q.; Ye, B.-C. *Anal. Chem.* **2013**, *85*, 11487−11493.
(12) Wang, M.; Fu, Z.; Li, B.; Zhou, Y.; Yin, H.; Ai, S. *Anal. Chem.* **2014**, *86*, 5606−5610.
(13) Tian, H.; Sun, Y.; Liu, C.; Duan, X.; Tang, W.; Li, Z. *Anal. Chem.* **2016**, *88*, 11384−11389.
(14) Lu, W.; Chen, Y.; Liu, Z.; Tang, W.; Feng, Q.; Sun, J.; Jiang, X. *ACS Nano* **2016**, *10*, 6685−6692.
(15) Castaneda, A. D.; Brenes, N. J.; Kondajji, A.; Crooks, R. M. *J. Am. Chem. Soc.* **2017**, *139*, 7657−7664.
(16) Tian, B.; Ma, J.; Qiu, Z.; Zardan Gomez de la Torre, T.; Donolato, M.; Hansen, M. F.; Svedlindh, P.; Stromberg, M. *ACS Nano* **2017**, *11*, 1798−1806.
(17) Zhang, P.; Wu, X.; Yuan, R.; Chai, Y. *Anal. Chem.* **2015**, *87*, 3202−3207.
(18) Bi, S.; Cui, Y.; Li, L. *Anal. Chim. Acta* **2013**, *760*, 69−74.
(19) Bi, S.; Yue, S.; Wu, Q.; Ye, J. *Chem. Commun.* **2016**, *52*, 5455−5458.
(20) Bi, S.; Xiu, B.; Ye, J.; Dong, Y. *ACS Appl. Mater. Interfaces* **2015**, *7*, 23310−23319.
(21) Dirks, R. M.; Pierce, N. A. *Proc. Natl. Acad. Sci. U. S. A.* **2004**, *101*, 15275−15278.
(22) Bi, S.; Yue, S.; Zhang, S. *Chem. Soc. Rev.* **2017**, *46*, 4281−4298.

DOI: 10.1021/acs.analchem.7b04930
Anal. Chem. XXXX, XXX, XXX−XXX

(23) Yin, P.; Choi, H. M. T.; Calvert, C. R.; Pierce, N. A. *Nature* **2008**, *451*, 318−323.
(24) Wu, H.; Liu, Y.; Wang, H.; Wu, J.; Zhu, F.; Zou, P. *Biosens. Bioelectron.* **2016**, *81*, 303−308.
(25) Yang, L.; Liu, C.; Ren, W.; Li, Z. *ACS Appl. Mater. Interfaces* **2012**, *4*, 6450−6453.
(26) Ge, Z.; Lin, M.; Wang, P.; Pei, H.; Yan, J.; Shi, J.; Huang, Q.; He, D.; Fan, C.; Zuo, X. *Anal. Chem.* **2014**, *86*, 2124−2130.
(27) Hou, T.; Li, W.; Liu, X.; Li, F. *Anal. Chem.* **2015**, *87*, 11368−11374.
(28) Zhang, L.; Wan, S.; Jiang, Y.; Wang, Y.; Fu, T.; Liu, Q.; Cao, Z.; Qiu, L.; Tan, W. *J. Am. Chem. Soc.* **2017**, *139*, 2532−2540.
(29) Gil, B.; Kahan-Hanum, M.; Skirtenko, N.; Adar, R.; Shapiro, E. *Nano Lett.* **2011**, *11*, 2989−2996.
(30) Bi, S.; Chen, M.; Jia, X.; Dong, Y.; Wang, Z. *Angew. Chem., Int. Ed.* **2015**, *54*, 8144−8148.
(31) Jung, C.; Ellington, A. D. *Acc. Chem. Res.* **2014**, *47*, 1825−1835.
(32) Lin, Y.; Xu, C.; Ren, J.; Qu, X. *Angew. Chem., Int. Ed.* **2012**, *51*, 12579−12583.
(33) Dong, H.; Meng, X.; Dai, W.; Cao, Y.; Lu, H.; Zhou, S.; Zhang, X. *Anal. Chem.* **2015**, *87*, 4334−4340.
(34) Bi, S.; Ye, J.; Dong, Y.; Li, H.; Cao, W. *Chem. Commun.* **2016**, *52*, 402−405.
(35) Janssen, B. M. G.; van Rosmalen, M.; van Beek, L.; Merkx, M. *Angew. Chem., Int. Ed.* **2015**, *54*, 2530−2533.
(36) Bi, S.; Chen, M.; Jia, X.; Dong, Y.; Wang, Z. *Angew. Chem., Int. Ed.* **2015**, *54*, 8144−8148.
(37) Wu, Z.; Wu, Z.-K.; Tang, H.; Tang, L.-J.; Jiang, J.-H. *Anal. Chem.* **2013**, *85*, 4376−4383.
(38) Yin, B.-C.; Liu, Y.-Q.; Ye, B.-C. *J. Am. Chem. Soc.* **2012**, *134*, 5064−5067.
(39) Qiu, X.; Zhang, H.; Yu, H.; Jiang, T.; Luo, Y. *Trends Biotechnol.* **2015**, *33*, 180−188.
(40) Jung, C.; Allen, P. B.; Ellington, A. D. *ACS Nano* **2017**, *11*, 8047−8054.
(41) Wang, W.-J.; Li, J.-J.; Rui, K.; Gai, P.-P.; Zhang, J.-R.; Zhu, J.-J. *Anal. Chem.* **2015**, *87*, 3019−3026.
(42) Wang, Y.; Jiang, L.-P.; Zhou, S.; Bi, S.; Zhu, J.-J. *ACS Appl. Mater. Interfaces* **2016**, *8*, 26532−26540.
(43) Wang, D.; Fu, Y.; Yan, J.; Zhao, B.; Dai, B.; Chao, J.; Liu, H.; He, D.; Zhang, Y.; Fan, C.; Song, S. *Anal. Chem.* **2014**, *86*, 1932−1936.
(44) Liu, Y.-Q.; Zhang, M.; Yin, B.-C.; Ye, B.-C. *Anal. Chem.* **2012**, *84*, 5165−5169.
(45) Yu, Y.; Chen, Z.; Shi, L.; Yang, F.; Pan, J.; Zhang, B.; Sun, D. *Anal. Chem.* **2014**, *86*, 8200−8205.
(46) Yang, C.; Dou, B.; Shi, K.; Chai, Y.; Xiang, Y.; Yuan, R. *Anal. Chem.* **2014**, *86*, 11913−11918.
(47) Hou, T.; Li, W.; Liu, X.; Li, F. *Anal. Chem.* **2015**, *87*, 11368−11374.
(48) Yang, C.; Shi, K.; Dou, B.; Xiang, Y.; Chai, Y.; Yuan, R. *ACS Appl. Mater. Interfaces* **2015**, *7*, 1188−1193.

DOI: 10.1021/acs.analchem.7b04930
Anal. Chem. XXXX, XXX, XXX−XXX